http://hdl.handle.net/2440/81293

Production of the H dibaryon via the (K^-, K^+) reaction on a ^{12}C target

R. Shyam,[1] O. Scholten,[2] and A. W. Thomas[3]

[1]*Saha Institute of Nuclear Physics, 1/AF Bidhan Nagar, Kolkata 700064, India and*
Physics Department, Indian Institute of Technology, Roorkee, India
[2]*Kernfysisch Versneller Instituut, University of Groningen, NL-9747 Groningen, The Netherlands*
[3]*Special Research Centre for the Subatomic Structure of Matter (CSSM) and ARC Centre of Excellence in Particle Physics at Terascale*
(CoEPP), School of Chemistry and Physics, University of Adelaide, Adelaide, South Australia 5005, Australia

We study the production of the stable six-quark H dibaryon via the (K^-, K^+) reaction on a ^{12}C target within a covariant effective Lagrangian model. The calculations are performed within a factorization approximation, in which the full production amplitude is written as a product of the amplitudes for the $K^- + p \rightarrow K^+ + \Xi^-$ and $\Xi^- + p \rightarrow H$ processes. The $K^+\Xi^-$ production vertex is described by excitation, propagation, and decay of Λ and Σ resonance states in the initial collision of a K^- meson with a target proton in the incident channel. The parameters of the resonance vertices are taken to be the same as those determined previously by describing the available data on total and differential cross sections for the $p(K^-, K^+)\Xi^-$ reaction within a similar model. The $\Xi^- + p \rightarrow H$ fusion process is treated within a quark model where the H dibaryon is considered as a stable particle. For the K^+ meson angle fixed at $0°$, the H production cross section is found to be about 2.9 $\mu b/sr$ for H mass just below the $\Lambda\Lambda$ threshold at a K^- beam momentum of 1.67 GeV/c. This is an order of magnitude larger than the value for this quantity reported earlier in calculations performed on a ^{3}He target using a different model for the cascade hyperon production. We have also calculated the beam momentum dependence of the H production cross section and the energy spectrum of the emitted K^+ meson.

I. INTRODUCTION

Within the quark-bag model, the H dibaryon, a six-quark [two up (u), two down (d), and two strange (s)] state with spin-parity $J^\pi = 0^+$ and isospin $I = 0$, was predicted to be a stable system with a mass about 80 MeV below the $\Lambda\Lambda$ threshold, some 35 years ago [1]. Later calculations, which included the center-of-mass (c.m.) [2] and pionic-cloud [3] corrections within this model, predicted this state to be much less bound or even unbound. Around the same time calculations performed within a quark-cluster model also found it unbound [4]. Since then a lot of experimental effort has gone into searching for the H dibaryon [see, e.g., the review [5] for references up to the year 2000 and Refs. [6,7] for more recent investigations done by Japan's National Laboratory for High Energy Physics (KEK) and the STAR Collaboration at the BNL Relativistic Heavy Ion Collider, respectively]. These studies have led to the conclusion that the existence of this system as a deeply bound object is highly unlikely. At the same time, the observation of the double-Λ hypernucleus $^6_{\Lambda\Lambda}$He (NAGARA event) and the precise determination of its binding energy at KEK in the experiment E373 [8] have put a lower limit of 2.224 GeV on the H-dibaryon mass at a 90% confidence level, which is just about 6.9 MeV below the $\Lambda\Lambda$ threshold.

The interest in the H dibaryon has been revived by the recent lattice quantum chromodynamics (LQCD) calculations of different groups. The NPLQCD [9] and HAL QCD [10] Collaborations have reported that the H particle is indeed bound at somewhat larger than physical pion masses. However, extrapolations of the calculations of these groups to the physical pion mass region suggest [11–13] that this particle is likely to be in either a very loosely bound state or an unbound state near the $\Lambda\Lambda$ threshold. In a very recent chiral constituent quark model calculation [14], the value extracted for the binding energy of the H particle has been found to be compatible with the restrictions imposed by the NAGARA event. These results together with the previous experiments [6] that give an upper limit for the cross section of the H production in the ^{12}C$(K^-, K^+\Lambda\Lambda)X$ reaction have led to a proposal to look for this particle in a future experiment [15] at the Japan Proton Accelerator Research Complex (JPARC) using a high-intensity K^- beam. This is expected to answer the long-standing question about the existence of the H dibaryon. Furthermore, with the measurement of the exclusive Ξ^- production in the $\gamma p \rightarrow K^+K^+\Xi^-$ reaction at the Jefferson Laboratory [16], a possibility has been opened for producing the H dibaryon with a photon beam.

The (K^-, K^+) reaction leads to the transfer of two units of both charge and strangeness to the target nucleus. Thus this reaction is one of the most promising ways of studying the production of $S = -2$ systems such as Ξ hypernuclei and the H dibaryon. Recently, the production of cascade hypernuclei via the (K^-, K^+) reaction on nuclear targets has been investigated within an effective Lagrangian model [17,18]. This is a new approach, where the $K^+\Xi^-$ production vertex is described by excitation, propagation, and decay of Λ and Σ resonance intermediate states in the initial collision of the K^- meson with a target proton in the incident channel. The Ξ^- hyperon gets captured into one of the nuclear orbits leading to the formation of the Ξ^- hypernucleus. In calculations of the Ξ^- hypernuclear production cross sections, one requires the bound state spinors for the proton hole and Ξ^- particle bound states. These were obtained by solving the Dirac equation with vector and scalar potential fields having Woods-Saxon

shapes. Their depths were fitted to the binding energies of the respective states. In Ref. [17] bound state spinors obtained in the quark-meson coupling (QMC) model [19] were also used. The cross sections for the hypernuclear production were found to be quite different from those calculated previously in Ref. [20].

In Ref. [17], the parameters at the resonance vertices were determined by describing the available data on total and differential cross sections for the elementary process $^{1}H(K^{-}, K^{+})\Xi^{-}$ within a similar effective Lagrangian model [17,21], where contributions were included from the s-channel and u-channel diagrams, which have as intermediate states Λ and Σ hyperons together with eight of their three- and four-star resonances [$\Lambda(1405)$, $\Lambda(1520)$, $\Lambda(1670)$, $\Lambda(1810)$, $\Lambda(1890)$, $\Sigma(1385)$, $\Sigma(1670)$, and $\Sigma(1750)$] with masses up to 2 GeV. It was observed that the total cross section of the $^{1}H(K^{-}, K^{+})\Xi^{-}$ reaction is dominated by the contributions from the $\Lambda(1520)$ (with $L_{IJ} = D_{03}$) resonance intermediate state. The region for beam momentum ($p_{K^{-}}$) below 2.0 GeV/c was found to be dominated by contributions from the s-channel graphs—the u-channel terms are dominant only in the region $p_{K^{-}} \leqslant 2.5$ GeV.

In this paper, we describe the production of the H dibaryon by the (K^{-}, K^{+}) reaction on ^{12}C as well as ^{3}He targets using a similar approach. The basic production mechanism considered in our work is depicted in Fig. 1, where this reaction proceeds in two steps. In the first step the $K^{+}\Xi^{-}$ production takes place by following the process as described above [see Fig. 1(a)], while in the second step the Ξ^{-} hyperon fuses with another proton of the residual nucleus to form the H dibaryon. A similar method was also used earlier in Refs. [22–24] in calculations of the production of this particle via (K^{-}, K^{+}). However, there are some differences between those calculations and the present work. In our method the amplitude for the $K^{-} + p_{1} \rightarrow K^{+} + \Xi^{-}$ reaction is calculated by employing the same method as that described in the previous paragraph. However, p_{1} is treated as a bound particle and in the calculations of the corresponding amplitude a bound state spinor is used for the initial proton state (p_{1}). Therefore, the dynamics of the $K^{+}\Xi^{-}$ production is intimately related to the wave function of the initial proton bound state [see Fig. 1(b)]. On the other hand, in the procedure of Refs. [22–24], the initial state is described by a product of the target wave function and the amplitude of the $K^{-} + p \rightarrow K^{+} + \Xi^{-}$ reaction. The latter is

determined from a parametrization of the sparsely available experimental 0° differential cross section for this reaction [see Fig. 1(a)] [23]. Furthermore, while in the previous models the numerical computations were limited to a very light ^{3}He target only, we have performed calculations also for a ^{12}C target. This makes it possible to compare our cross sections directly to the existing experimental results and to make predictions for future measurements.

As discussed in Ref. [23], there may be several higher-order processes through which the H-dibaryon production can proceed. They lead to the H dibaryon via $\Lambda\Lambda$ or $\Sigma\Sigma$ fusion. The latter are produced via the following reactions: $K^{-} + p \rightarrow \Lambda(\Sigma) + \pi$; $\pi + p \rightarrow \Lambda(\Sigma) + K^{+}$ or $K^{-} + p \rightarrow K^{+} + \Xi^{-}$; $\Xi^{-} + p \rightarrow \Lambda\Lambda(\Sigma\Sigma)$. It is shown in Ref. [23] that the contributions of such terms are not expected to be large and they can be ignored. Therefore, like these authors, we have also neglected such diagrams in our study.

In Ref. [25], an alternative scheme of H production has been discussed in which a tagged Ξ^{-} hyperon is first produced on a hydrogen target via the reaction $K^{-} + p \rightarrow K^{+} + \Xi^{-}$; it is then slowed down by passing through a moderator. After moderation, the slow $\Xi^{-}s$ are captured in a second target into an atomic orbit, and the H is subsequently produced via, e.g., the processes, $(\Xi^{-} p)_{atom} \rightarrow H + \gamma$, $(\Xi^{-} d)_{atom} \rightarrow H + n$, and $(\Xi^{-4}He)_{atom} \rightarrow H + t$. To ensure that an H with sharply defined mass is indeed produced, the K^{+} and monoenergetic γ, neutron, or triton should be detected in coincidence. These authors have estimated the branching ratios (R) of the three H-formation reactions relative to the total decay widths of the Ξ^{-} atoms. It has been found that R has a sizable value (in excess of 0.5) for $(\Xi^{-}d)$ and $(\Xi^{-4}He)$ atoms if H mass (m_{H}) is very close to the $\Lambda\Lambda$ threshold. Therefore, these processes have their merit for such values of m_{H}. However, these estimates of R are based on very poorly known amplitudes for the transitions $\Xi N \rightarrow \Xi N$, $\Lambda\Lambda$, and $\Sigma\Sigma$ at low momentum and are strongly dependent on the models chosen to calculate them. The virtue of the $A(K^{-}, K^{+})HB$ reaction studied in this paper is that H production occurs through a second-order process within a single nuclear target where all the components of the total amplitude can be calculated relatively more reliably. Furthermore, unlike the Ξ^{-} atom method, there are no weak decay losses of Ξ^{-} during moderation to low momentum.

II. FORMALISM

We have followed the procedure and notations of Ref. [26] in deriving the formulas for the invariant cross section of the $K^{-} + A \rightarrow K^{+} + H + B$ reaction, which can be written as (see, e.g., Ref. [27])

$$d\sigma = \frac{m_{H}m_{A}m_{B}}{\sqrt{[(p_{K} - p_{A})^{2} - m_{K^{-}}^{2} - m_{A}^{2}]}} \frac{1}{4(2\pi)^{5}} \delta^{4}(P_{f} - P_{i})|A_{fi}|^{2}$$

$$\times \frac{d^{3}p_{K^{+}}}{E_{K^{+}}} \frac{d^{3}p_{B}}{E_{B}} \frac{d^{3}p_{H}}{E_{H}}, \quad (1)$$

where A_{fi} represents the total amplitude; P_{i} and P_{f} represent the sum of all the momenta in the initial and final states, respectively; and m_{H}, m_{A}, and m_{B} represents the masses of
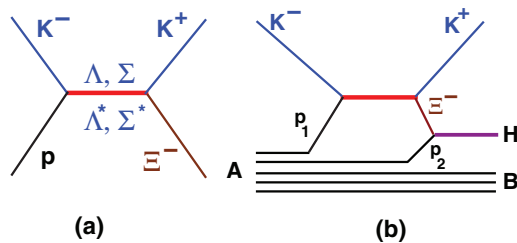

FIG. 1. (Color online) Graphical representation of the model used to describe the $^{1}H(K^{-}, K^{+})\Xi^{-}$ [Fig. 1(a)] and $A(K^{-}, K^{+})HB$ reactions [Fig. 1(b)], where A represents the target nucleus while $B = (A - 2)$ represents the residual nucleus. In Fig. 1(a), Λ^{*} and Σ^{*} represent the Λ and Σ resonance states, respectively.

the *H* dibaryon and nuclei *A* and *B*, respectively. The cross sections in the laboratory or c.m. systems can be written from this equation by imposing the relevant conditions. Summations over final spin states and averages over initial spin states are implied in $|A_{fi}|^2$.

Following the factorization approximation of Ref. [23], the total amplitude A_{fi} is written as the product of the amplitudes for the processes $K^- + p_1 \rightarrow K^+ + \Xi^-$ [$M(K^- + p_1 \rightarrow K^+ + \Xi^-)$] and $\Xi^- + p_2 \rightarrow H$ [$F(\Xi^- + p_2 \rightarrow H)$] [see Fig. 1(b)]. We write

$$
A_{fi} = \int \frac{d^4 p_1}{(2\pi)^4} \int \frac{d^4 p_2}{(2\pi)^4} \delta(p_1 + p_{K^-} - p_{K^+} - p_{\Xi^-})
$$

$$
\times \delta(p_H - p_{\Xi^-} - p_2) \left[\sum_{Y^*} M(K^- + p_1 \right.
$$

$$
\left. \rightarrow K^+ + \Xi^-) \right] F(\Xi^- + p_2 \rightarrow H), \qquad (2)
$$

where p_{K^-}, p_{K^+}, and p_{Ξ^-} are the four momenta of the incoming and outgoing kaons and the Ξ^- hyperon, respectively. In Eq. (2) the δ functions represent the momentum-energy conservation at various vertices. Some of them can be used to reduce the dimensionality of the integrations in this equation.

The amplitude $M(K^- + p_1 \rightarrow K^+ + \Xi^-)$, where the summation is done over all the resonance intermediate states Y^* as described above, has been determined by following the method discussed in Ref. [17]. The effective Lagrangians, the corresponding coupling constants and the form factors for the resonance-kaon-baryon vertices, the propagators for the intermediate resonances and the bound state and free-space wave functions for the bound proton p_1 and the intermediate Ξ^- hyperon, respectively, as used in the calculations of the amplitude M, are discussed in the following.

The effective Lagrangians for the resonance-kaon-baryon vertices for spin-$\frac{1}{2}$ and spin-$\frac{3}{2}$ resonances are taken as

$$
\mathcal{L}_{\mathrm{KBR}_{1/2}} = -g_{\mathrm{KBR}_{1/2}} \bar{\psi}_{R_{1/2}} \left[\chi i \Gamma \varphi_K + \frac{(1-\chi)}{M} \Gamma \gamma_\mu (\partial^\mu \varphi_K) \right] \psi_B,
$$
$$(3)$$

$$
\mathcal{L}_{\mathrm{KBR}_{3/2}} = \frac{g_{\mathrm{KBR}_{3/2}}}{m_K} \bar{\psi}^\mu_{R_{3/2}} \partial_\mu \phi_K \psi_B + \mathrm{H.c.}, \qquad (4)
$$

with $M = (m_R \pm m_B)$, where the upper sign corresponds to an even-parity and the lower sign to an odd-parity resonance with *B* representing either a nucleon or a Ξ hyperon and *R* representing a resonance. The spinors ψ_B are defined later on. The operator Γ is γ_5 (1) for an even-parity (odd-parity) resonance. The parameter χ controls the admixture of pseudoscalar and pseudovector components. The value of this parameter is taken to be 0.5 for the Λ^* and Σ^* states, but 0 for the Λ and Σ states, implying pure pseudovector couplings for the corresponding vertices, in agreement with Refs. [27,28]. The Lagrangian for spin-$\frac{3}{2}$, as given by Eq. (4), corresponds to that of a pure Rarita-Schwinger form that has been used in all previous calculations of the hypernuclear production reactions within a similar effective Lagrangian model [28–31]. The values of the vertex parameters were taken to be the same as those given in Ref. [17].

Similar to Refs. [17,21], we have used the following form factor at various vertices,

$$
F_m(s) = \frac{\lambda^4}{\lambda^4 + (s - m^2)^2}, \qquad (5)
$$

where *m* is the mass of the propagating particle. The cutoff parameter λ is taken to be 1.2 GeV, the same as that used in Refs. [17,21].

The two interaction vertices of Fig. 1 are connected by a resonance propagator. For the spin-1/2 and spin-3/2 resonances, the propagators are given by

$$
\mathcal{D}_{R_{1/2}} = \frac{i\left(\gamma_\mu p^\mu + m_{R_{1/2}}\right)}{p^2 - \left(m_{R_{1/2}} - i\Gamma_{R_{1/2}}/2\right)^2} \qquad (6)
$$

and

$$
\mathcal{D}^{\mu\nu}_{R_{3/2}} = -\frac{i\left(\gamma_\lambda p^\lambda + m_{R_{3/2}}\right)}{p^2 - \left(m_{R_{3/2}} - i\Gamma_{R_{3/2}}/2\right)^2} P^{\mu\nu}, \qquad (7)
$$

respectively. In Eq. (7) we have defined

$$
P^{\mu\nu} = g^{\mu\nu} - \frac{1}{3}\gamma^\mu \gamma^\nu - \frac{2}{3m^2_{R_{3/2}}} p^\mu p^\nu
$$

$$
+ \frac{1}{3m_{R_{3/2}}} (p^\mu \gamma^\nu - p^\nu \gamma^\mu). \qquad (8)
$$

In Eqs. (6) and (7), $\Gamma_{R_{1/2}}$ and $\Gamma_{R_{3/2}}$ define the total widths of the corresponding resonances. We have ignored any medium modification of the resonance widths while calculating the amplitude *M*, because information about such changes is scarce and uncertain.

The bound proton wave function [$\psi(p_1)$] is a four component Dirac spinor, which is the solution of the Dirac equation for a bound state problem in the presence of external scalar and vector potential fields. This is written as

$$
\psi(p_1) = \delta(p_{10} - E_1) \begin{pmatrix} f(k_1) \mathcal{Y}^{m_j}_{\ell 1/2 j}(\hat{p}_1) \\ -ig(k_1) \mathcal{Y}^{m_j}_{\ell' 1/2 j}(\hat{p}_1) \end{pmatrix}, \qquad (9)
$$

In our notation p_1 represents a four-momentum, and $\boldsymbol{p_1}$ a three-momentum. The magnitude of $\boldsymbol{p_1}$ is represented by k_1, and its directions are represented by $\hat{p}_1$. p_{10} represents the timelike component of momentum p_1. In Eq. (9) $f(k_1)$ and $g(k_1)$ are the radial parts of the upper and lower components of the spinor $\psi(p_1)$, $\mathcal{Y}^{m_j}_{\ell 1/2 j}$ are the coupled spherical harmonics

$$
\mathcal{Y}^{m_j}_{\ell 1/2 j} = \langle \ell m_\ell 1/2 \mu_i | j m_j \rangle Y_{\ell m_\ell}(\hat{p}_1) \chi_\mu, \qquad (10)
$$

and $\ell' = 2j - \ell$, with ℓ and j being the orbital and total angular momenta, respectively. *Y* represents the spherical harmonics, and χ_μ the spin space wave function of a spin-$\frac{1}{2}$ particle.

We assume that the nucleon bound state has a pure single particle-hole configuration with the core remaining inert. To simplify the nuclear structure problem, we assume that the initial bound proton (p_1) is picked up from the $1p_{3/2}$ orbit with a binding energy of 15.96 MeV. Although, it is straightforward to include also those cases where the participating proton occupies both *p* and *s* orbits. However, picking a proton from the *s* state will lead to an unstable residual nucleus in the present case (see, e.g., Refs. [32,33]). Treatment of such systems is beyond the scope of this work.

The free-space spinor for the Ξ^- hyperon is written as

$$\Psi(p_{\Xi^-}) = \delta(p_{\Xi^-_0} - E_{\Xi^-})\sqrt{\frac{E_{\Xi^-} + m_{\Xi^-}}{2m_{\Xi^-}}}\left(\begin{array}{c}\chi_\mu \\ \frac{\sigma \cdot \boldsymbol{p}_{\Xi^-}}{E_{\Xi^-}+m_{\Xi^-}}\chi_\mu\end{array}\right),$$

(11)

where $p_{\Xi^-_0}$ is the timelike component of the momentum p_{Ξ^-}. Because our calculations are carried out in momentum space, they include all the nonlocalities in the production amplitudes that arise from the resonance propagators.

We have used a plane wave approximation to describe the relative motion of kaons in the incoming and outgoing channels. However, the distortion effects are partially accounted for by introducing a reduction factor of 4 to the overall cross sections, as described in Refs. [17,20]. It should be mentioned that this factor corresponds to absorption effects on only the K^- and K^+ wave functions. There could still be the distortion effect on the H-B relative motion in the final channel, which is ignored here.

For calculating the amplitude $F(\Xi^- + p_2 \rightarrow H)$, we follow the same procedure as described in Ref. [23]. In this method, the H dibaryon is treated as a bound particle with a mass m_H; however, its six-quark structure is taken into account. This implies that the three-quark internal structures of the Ξ^- hyperon and the proton p_2 [see Fig. 1(b)] also have to be invoked as the formation of H is thought of in terms of the fusion of two three-quark bags (Ξ^- and p_2). The amplitude F is calculated by taking the overlap of the internal wave functions of H, Ξ^-, and p_2, which are described by a Gaussian approximation (see Ref. [22]). The final result for the amplitude F is given by

$$F(\Xi^- + p_2 \rightarrow H)$$
$$= \Gamma_0\left(\frac{2R_pR_H}{R_H^2 + R_p^2}\right)^3\left(\frac{2R_{\Xi^-}R_H}{R_H^2 + R_{\Xi^-}^2}\right)^3$$
$$\times \left(\frac{2R_H^2}{3\pi}\right)^{3/4}\exp\left[-\frac{R_H^2}{12}(\boldsymbol{p}_2 - \boldsymbol{p}_{\Xi^-})^2\right], \quad (12)$$

where the factor Γ_0 arises from the color-flavor-spin recoupling as defined in Ref. [23]. Its value is $\sqrt{1/20}$. The values of the oscillator parameters R_p, R_{Ξ^-}, and R_H have been taken to be 0.83, 0.73, and 0.95 fm, respectively. The chosen value of R_p reproduces the root-mean-square (rms) radius of the proton, while the value of R_{Ξ^-} comes from the quark-bag model relation between the proton bag radius and that of the Ξ^-. The bag radius of the H dibaryon is about 20% larger than that of the proton (see, e.g., Refs. [2,3]). Therefore, we have increased the value of R_H over R_p accordingly. In deriving Eq. (12), the normalizations of the baryon wave functions have been made consistent with those of the amplitude M.

III. RESULTS AND DISCUSSION

A. Initial bound state spinors

The initial bound state spinors in momentum space are obtained by Fourier transformation of the corresponding coordinate space spinors, which are the solutions of the
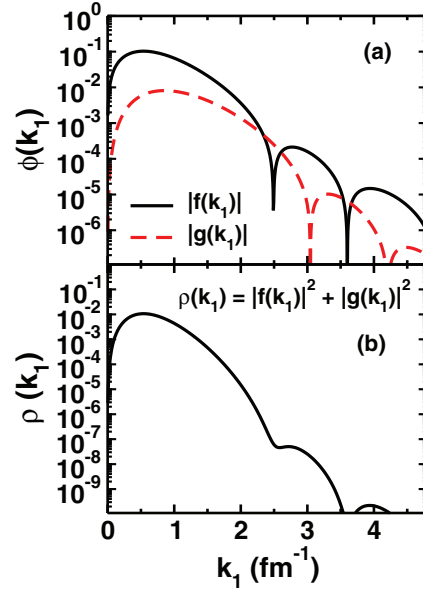

FIG. 2. (Color online) (a) Momentum space spinors [$\phi(k_1)$] for the $1p_{3/2}$ nucleon orbit in ^{12}C. $f(k_1)$ and $g(k_1)$ are the upper and lower components of the spinor, respectively. (b) Momentum distribution [$\rho(k_1)$] for the same state calculated with the wave function shown in panel (a).

Dirac equation with potential fields consisting of an attractive scalar part (V_s) and a repulsive vector part (V_v), both having Woods-Saxon shapes. For fixed geometry parameters (radius and diffuseness) we search for the depths of these potentials to reproduce the binding energy of the respective state. With our choice of quantum numbers and the binding energy for the p_1 proton state, the resulting depths were 382.6 and −472.3 MeV, respectively, for the fields V_v and V_s, with the radius and diffuseness parameters of 0.983 and 0.606 fm, respectively, for both. To show the momentum spread of the corresponding spinors, we have displayed in Figs. 2(a) and 2(b) the spinors $|f(k_1)|$ and $|g(k_1)|$ and the momentum distribution $\rho(k_1) = |f(k_1)|^2 + |g(k_1)|^2$ as a function of momentum k_1, respectively. It may be noted that spinors calculated in this way provide a good description of the nucleon momentum distribution for the p-shell nucleons as shown in Ref. [34]. It should further be added here that these spinors are the same as those used in Refs. [17,30] to describe the productions of the Λ and Ξ^- hypernuclei via the (γ, K^+) and (K^-, K^+) reactions, respectively, on a ^{12}C target.

B. Dibaryon production cross sections

The method discussed above has been used to study the ^{12}C(K^-, K^+)H ^{10}Be reaction. In Fig. 3, we show the results for the differential cross section $d\sigma/d\Omega_{K^+}$ at the K^+ angle of 0° and the beam momentum ($p_{K^-}^{\rm lab}$) of 1.67 GeV/c, as a function of the rest mass of the H dibaryon. We note that the cross section decreases uniformly as m_H approaches the $\Lambda\Lambda$ threshold (indicated by an arrow), where we stopped the calculations because our method treats the H as a bound particle. In Ref. [6], the upper limit of the production cross
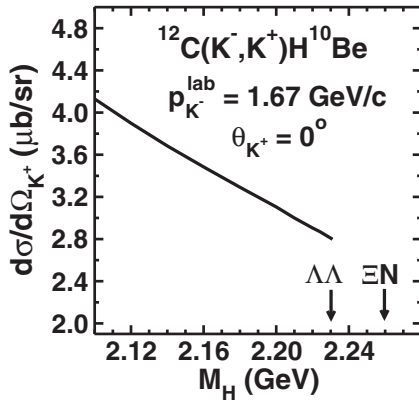
FIG. 3. Differential cross section $d\sigma/d\Omega_{K^+}$ at $\theta_{K^+} = 0°$ for H production in the $^{12}C(K^-, K^+)H \, ^{10}Be$ reaction at the beam momentum of 1.67 GeV/c, as a function of H-dibaryon mass. The $\Lambda\Lambda$ and ΣN thresholds are shown by arrows as indicated.

section of H with a mass range between $\Lambda\Lambda$ and ΣN thresholds (also indicated in Fig. 2 by an arrow) has been estimated to be 2.1 ± 0.6 (stat.) ± 0.1 (syst.) $\mu b/sr$ at a 90% confidence level, in a measurement of the $^{12}C(K^-, K^+)\Lambda\Lambda X$ reaction at the beam momentum of 1.67 GeV/c where the K^+ meson was confined mostly in the forward directions. In Fig. 3, the cross section at the $\Lambda\Lambda$ threshold is comparable to this value.

In Fig. 4(a), we show the beam momentum dependence of the cross section $d\sigma/d\Omega_{K^+}$ for the $^{12}C(K^-, K^+)H \, ^{10}Be$ reaction. The result in this figure mirrors the beam momentum dependence of the same cross section in the Ξ^- hypernuclear production reaction $^{12}C(K^-, K^+)^{12}_{\Xi^-}Be$, shown in Refs. [17,18]. The cross section peaks near the $p_{K^-}^{lab}$ value of about 1.05 GeV/c, which is approximately 0.30 GeV/c away from the production threshold for this reaction (0.735 GeV/c). This is similar to the case of the hypernuclear production reactions, as mentioned above, where the threshold is 0.761 GeV/c. We recall that in the case of the 0° differential cross section for the elementary production reaction $^1H(K^-, K^+)\Xi^-$, the peak also occurs at about 0.35–0.40 GeV/c above the corresponding production threshold (see Refs. [17,21]).
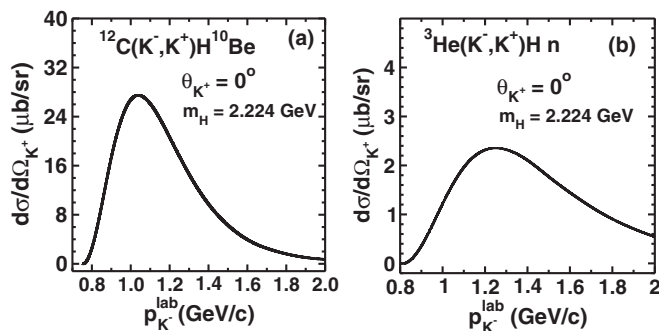

FIG. 4. Differential cross section $d\sigma/d\Omega_{K^+}$ at $\theta_{K^+} = 0°$ for the reactions $^{12}C(K^-, K^+)H \, ^{10}Be$ (a) and $^3He(K^-, K^+)H \, n$ (b) as a function of the laboratory beam momentum $p_{K^-}^{lab}$ corresponding to an H-dibaryon mass of 2.224 GeV.

The magnitude of the cross section near the peak position in Fig. 4(a) is about an order of magnitude larger than that at the beam momentum of 1.8 GeV/c. This is similar to that seen in Refs. [17,18] for the $^{12}C(K^-, K^+)^{12}_{\Xi^-}Be$ reaction. Moreover, the peak cross section of the present reaction is smaller than that of the elementary production reaction by roughly a factor of 2. However, it is about an order of magnitude larger than that of the $^{12}C(K^-, K^+)^{12}_{\Xi^-}Be$ reaction. This is the consequence of the extremely restricted phase space available in the latter case that has a two-body final state involving a bound system.

It is evident that in our model the bound state spinors in the initial state are calculated within a mean-field approximation; therefore, its application to a lighter target like ^3He should be less valid. Nevertheless, in order to have a direct comparison with the results shown in Refs. [23,24] for the $^3He(K^-, K^+)Hn$ reaction, we have calculated the beam momentum dependence of the cross section $d\sigma/d\Omega_{K^+}$ at $\theta_{K^+} = 0°$ for this reaction within our model. The initial bound proton in this case is from the $1s_{1/2}$ orbit with a binding energy of 5.49 MeV. The corresponding spinors were determined by a procedure similar to that described above using the same geometry parameters. The depths of the fields V_v and V_s were 210.41 and -259.76 MeV, respectively. The spinors were normalized to reproduce the experimental rms radius of ^3He (1.88 fm). Our results for the 0° cross section $d\sigma/d\Omega_{K^+}$ for the corresponding H production reaction are shown in Fig. 4(b). We note that the maximum of the cross section in this case is at a $p_{K^-}^{lab}$ value around 1.20 GeV/c. The shift in the peak position to a larger $p_{K^-}^{lab}$ as compared to that in Fig. 4(a) can be understood from the fact that the threshold for the $^3He(K^-, K^+)Hn$ reaction (≈ 0.80 GeV/c) is larger than that of the reaction on a ^{12}C target.

It should be mentioned here that in Refs. [23,24] the corresponding cross section peaks at $p_{K^-}^{lab} \approx 1.75$ GeV/c, which coincides exactly with the peak position of the 0° $d\sigma/d\Omega_{K^+}$ of the elementary reaction $^1H(K^-, K^+)\Xi^-$ used by these authors in their calculations. In this context two points are worth noticing. First, the peak in the elementary production cross section calculated in our model occurs at a lower $p_{K^-}^{lab}$ (around 1.5 GeV/c) as shown in Refs. [17,18,21]. Second, because in our calculations of the $A(K^-, K^+)HB$ reactions, the $K^+\Xi^-$ production amplitudes are obtained by considering the initial proton as a particle bound in one of the orbits of the target nucleus, the threshold effects pull back the peak position in the $^3He(K^-, K^+)Hn$ reaction to a $p_{K^-}^{lab}$ value lower than that of the elementary reaction. This effect is not seen in results shown in Refs. [23,24] due to their particular choice of the initial state as discussed in the previous section.

Near $p_{K^-}^{lab} \approx 1.75$ GeV/c, the magnitude of our cross section is about 0.95 $\mu b/sr$. This is larger than those of Refs. [23] and [24], by factors of 2–3 and 1.5–2.0, respectively. This can be attributed to the difference in the model used to calculate the $K^+\Xi^-$ production amplitudes by these authors as compared to that of ours.

Looking at the results for the H production reactions shown in Figs. 4(a) and 4(b), we notice that the ratio (R_{cs}) of the magnitudes of the cross sections for the ^{12}C and the ^3He targets is greater than one for all the beam momenta. However, the
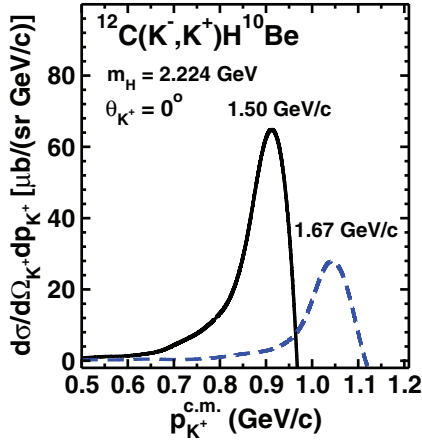
FIG. 5. (Color online) Double differential cross section $d\sigma/d\Omega_{K^+}dp_{K^+}$ at $\theta_{K^+} = 0^\circ$ for the ^{12}C$(K^-, K^+)H$ ^{10}Be reaction as a function of the c.m. momentum $p_{K^+}^{\text{c.m.}}$ of the K^+ meson at the $p_{K^-}^{\text{lab}}$ values of 1.50 GeV/c (solid line) and 1.67 GeV/c (dashed line). The H mass is fixed at 2.224 GeV for both the cases.
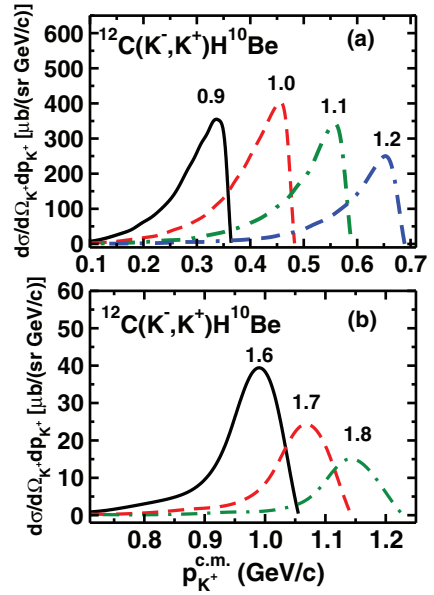

FIG. 6. (Color online) (a) Double differential cross section $d\sigma/d\Omega_{K^+}dp_{K^+}$ at $\theta_{K^+} = 0^\circ$ for the ^{12}C$(K^-, K^+)H$ ^{10}Be reaction as a function of the c.m. momentum $p_{K^+}^{\text{c.m.}}$ of the K^+ meson for $p_{K^-}^{\text{lab}}$ values of 0.9 GeV/c (solid line), 1.0 GeV/c (dashed line), 1.1 GeV/c (dashed-dotted line), and 1.2 GeV/c (dashed-dashed-dotted line). (b) The same as in panel (a) for $p_{K^-}^{\text{lab}}$ values of 1.6 GeV/c (solid line), 1.7 GeV/c (dashed line), and 1.8 GeV/c (dashed-dotted line). The H mass is fixed at 2.224 GeV for all the cases.

point to note is that this ratio is beam momentum dependent. While near peak positions the value of R_{cs} is about 10, in the tail region ($p_{K^-}^{\text{lab}} > 1.6$ GeV/c) it varies between 4 and 2. From Eq. (1), it is evident that the mass terms already make the phase-space factor of the reaction on a ^{12}C target larger than that on ^{3}He by nearly an order of magnitude. Of course, there is a strong dependence of the product of the rest of the phase space and the modulus square of the amplitudes on various momenta. They combine with the mass terms of the phase space to produce the target mass dependence seen in Figs. 4(a) and 4(b). Results shown in Fig. 4(a) may affect some of the conclusions of Refs. [35,36] where the cross sections for the H production via the (K^-, K^+) reaction on a ^{12}C target have been estimated from an extrapolation of the results on the ^{3}He target reported in Ref. [23].

In Fig. 5, we show the double differential cross sections $d\sigma/d\Omega_{K^+}dp_{K^+}$ for the same reaction as in Fig. 4(a) at $p_{K^-}^{\text{lab}}$ values of 1.5 and 1.67 GeV/c and at the K^+ c.m. angle $\theta_{K^+} = 0^\circ$, as a function of the c.m. momentum of K^+ meson ($p_{K^+}^{\text{c.m.}}$). The c.m. frame refers to that of the $K^- + ^{12}$C system. The H-dibaryon mass was taken to be 2.224 GeV in both cases. It is seen that these cross sections are peaked very close to the kinematically allowed maximum of $p_{K^+}^{\text{c.m.}}$ ($p_{K^+}^{\text{c.m.,max}}$) and have narrow widths of about 90 MeV. The peaking of the cross section near $p_{K^+}^{\text{c.m.,max}}$ can be understood from the fact that the quark-fusion amplitude is largest for smallest values of Ξ^- momenta, which happens for the maximum value of the K^+ momentum.

In Fig. 6, $d\sigma/d\Omega_{K^+}dp_{K^+}$ is shown for several beam momenta ($p_{K^-}^{\text{lab}}$) for the same reaction as in Fig. 5. It is observed that the peaking in the K^+ momentum spectra very close to $p_{K^+}^{\text{c.m.,max}}$ is found in all the cases. As $p_{K^-}^{\text{lab}}$ increases $p_{K^+}^{\text{c.m.,max}}$ shifts to higher values and so does the peak position in the corresponding cross section. However, the widths of the distributions remain unaltered. Nevertheless, at very large values of the $p_{K^-}^{\text{lab}}$ [in Fig. 6(b)] the distributions tend to become more symmetric and the peak positions are at relatively somewhat lower values of $p_{K^+}^{\text{c.m.}}$ as compared to those at lower

$p_{K^-}^{\text{lab}}$. This is mainly due to more dominant role of the phase space component of the cross section at these higher values of $p_{K^-}^{\text{lab}}$. The magnitudes of the peak cross sections at various values of $p_{K^-}^{\text{lab}}$ have a trend that is consistent with that seen in Fig. 4(a).

To understand more clearly the cause for the narrow width of the K^+ momentum spectra, we display in Fig. 7 decomposition of the cross section $d\sigma/d\Omega_{K^+}dp_{K^+}$ into phase-space-only (dotted line), Ξ^--production-only (dashed line), and quark-fusion-only (solid line) components. The $p_{K^-}^{\text{lab}}$ is chosen to be 1.67 GeV/c and various curves in this figure are normalized to the same maximum value. The three-body phase-space component is broad and has a peak at K^+ momentum much below the corresponding $p_{K^+}^{\text{c.m.,max}}$ ($\sim$1.05 GeV). Therefore, if the shape of the K^+ momentum spectrum were estimated from the pure phase space, it would have a much more spread-out distribution. Although the Ξ^--production-only component is narrower than the phase-space-only component, it is still broader than the cross sections shown in Fig. 5. On the other hand, the quark-fusion-only component has a narrower width that is similar to that of the final cross section. Because of the domination of this component in the cross section near the peak position, the shape of the K^+ spectrum is governed by it in the region of interest. The magnitude of the width of the K^+ momentum spectrum obtained by us can be understood from simple kinematical arguments as discussed in the Appendix.

It is important to compare the narrow peak in the K^+ spectrum for the H production reaction with that in the
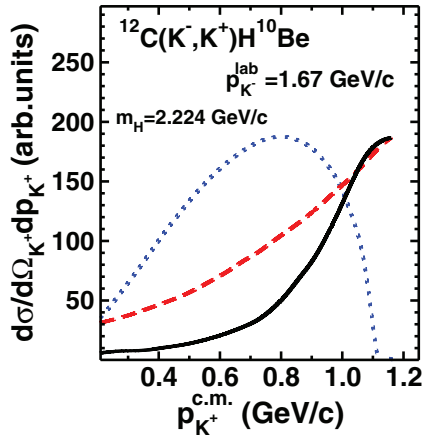
FIG. 7. (Color online) The phase-space-only (dotted line), Ξ^--production-only (dashed line), and $\Xi^- + p \rightarrow H$ fusion-only (solid line) components of the differential cross section $d\sigma/d\Omega_{K^+}dp_{K^+}$ at $\theta_{K^+} = 0^\circ$ for the $^{12}C(K^-, K^+)H\,^{10}Be$ reaction as a function of momentum $p_{K^+}^{c.m.}$ at the $p_{K^-}^{lab}$ value of 1.67 GeV/c. The H mass is fixed at 2.224 GeV. All the curves are normalized to the same peak cross section.

momentum spectrum of the K^+ for background processes like the $^{12}C(K^-, K^+)^{10}Be\ \Xi^- p$ reaction. The results of the calculations for this type of background reaction on a ^{3}He target are discussed in Refs. [23,24]. It is shown there that such processes have a relatively larger magnitude and a much broader width of the K^+ momentum spectrum. Therefore, it should be possible to separate the H production from the $\Xi^- p$ background as the peak of the K^+ spectrum in the latter reaction would be well separated from that for H production. There is another potential source of background, namely, the possible production of two Λ hyperons in the interaction of the Ξ^- with proton p_2. The probability for such processes, initiated by the Ξ^- particle in a nuclear bound state, has been calculated in Refs. [37–39]. These calculations suggest that the relative probability for the $\Xi^- + p \rightarrow \Lambda\Lambda$ reaction involving a free Ξ^- particle may not be more than 10–20%.

IV. SUMMARY AND CONCLUSIONS

In summary, we have studied the production of the stable six-quark H dibaryon, via the (K^-, K^+) reaction on a ^{12}C target within an effective Lagrangian model. We have also made some calculations for this reaction on a ^{3}He target. The model assumes this reaction to proceed in two steps. In the first step, a Ξ^- hyperon and a K^+ meson are produced in the initial collision of the K^- meson with a proton bound in the target. In the second step, the Ξ^- hyperon fuses with another target proton to produce the H dibaryon. Our method differs from the previous calculations of this reaction, which use a similar two-step approach, in several ways. In our work the $\Xi^- + K^+$ production amplitude has been calculated by excitation, propagation, and decay of Λ and Σ hyperon resonance intermediate states in the initial collision of the K^- meson with a target proton. The vertex parameters (the coupling constants and the form factors) at the resonance

vertices have been taken to be the same as those fixed earlier by describing both the total and the differential cross sections of the elementary $^1H(K^-, K^+)\Xi^-$ reaction within a similar model. The same parameters were also used recently in the calculations of the Ξ hypernuclei. The bound proton spinors have been obtained by solving the Dirac equation with vector and scalar potential fields having Woods-Saxon shapes. Their depths are fitted to the binding energies of the respective states. In the previous studies of this reaction, the $\Xi^- + K^+$ production amplitudes were obtained from a parametrization of the scantily known experimental differential cross sections of the $^1H(K^-, K^+)\Xi^-$ reaction at 0°. Moreover, while we have applied our model to compute cross sections for the (K^-, K^+) reaction on ^{12}C as well as ^{3}He targets, in the previous models the numerical calculations were limited only to a ^{3}He target.

In our study, the H-dibaryon production cross section in the $^{12}C(K^-, K^+)\ H\,^{10}Be$ reaction at the K^- beam momentum of 1.67 GeV/c, and for an H mass very close to the $\Lambda\Lambda$ threshold, is found to be comparable to the upper limit of the H production cross section estimated just above this threshold with a 90% confidence level in a study of the $^{12}C(K^-, K^+)\Lambda\Lambda X$ reaction at the same beam momentum.

We notice that the differential cross section of the $^{12}C(K^-, K^+)H\,^{10}Be$ reaction for observing K^+ at 0° peaks around the beam momentum of 1.05 GeV/c. This mirrors the beam momentum dependence of the corresponding cross section in the Ξ^- hypernuclear production reaction $^{12}C(K^-, K^+)^{12}_{\Xi^-}Be$. In case of the ^{3}He target the peak position shifts to a higher beam momentum of 1.20 GeV/c because the threshold of the reaction on this target is larger than that on ^{12}C. The peak positions in these cross sections are above the production thresholds of the corresponding reactions by almost the same amount as the position of the maximum is above the corresponding threshold in the 0° differential cross section of the elementary $^1H(K^-, K^+)\Xi^-$ reaction. In our model, the magnitudes of cross sections of the reaction on a ^{12}C target are larger than those on ^{3}He by an order of magnitude for beam momenta around the respective peak positions. However, in the tail region (for $p_{K^-}^{lab}$ larger than 1.6 GeV/c) the difference between the two is within factors of 4–2.

The K^+ momentum spectrum has a peak very close to the kinematically allowed maximum K^+ momentum and its width is narrow (about 90 MeV/c). This feature is independent of the K^- beam momentum. It is also shown here that a larger H production cross section is expected in experiments performed at beam momenta around 1 GeV/c. The background process such as the K^+ recoiling against the continuum $\Xi^- p$ pair [23,24] has a relatively larger magnitude and broader width of the K^+ momentum spectrum and therefore can be rather cleanly separated from the H signal.

APPENDIX: KINEMATICS OF *H*-DIBARYON PRODUCTION

To obtain more insight into the kinematical factors that determine the structure of the spectrum we have performed a very simple calculation where the focus is on the kinematics. We use a convention where the incoming K^- momentum (p_{K^-}), is taken in the z direction like that of the outgoing K^+ (p_{K^+}). Simplifying the reaction dynamics to a minimum the expression for the cross section can be expressed as an integral over the longitudinal (z) component, p_r^l, of the recoil momentum, p_r, of the ($A-2$) residual nucleus,

$$\sigma_r(p_{K^+}) = \int dp_r^l \rho_r(p_r) p_r^\perp, \qquad (A1)$$

where $p_r^\perp$ is the perpendicular (x) component of the recoil momentum, thus $p_r = \sqrt{(p_r^l)^2 + (p_r^\perp)^2}$. In Eq. (A1) the overlap integral is written as

$$\rho_r(p_r) = \int d^3\boldsymbol{p}_1 \, \rho_1(k_1) \, \rho_2(k_2) \, \rho_H(\Delta p_H), \qquad (A2)$$

where $\boldsymbol{p}_2 = \boldsymbol{p}_1 - \boldsymbol{p}_r$ by momentum conservation. We have followed the notations for momenta of bound protons as described after Eq. (9) in the main text. The probability density for a proton with momentum k_i in the nucleus A is parametrized as

$$\rho_i(k_i) = k_i e^{-(k_i/w_1)^2}/w_1^2, \qquad (A3)$$

which fits reasonably well the probability distribution given in Fig. 2 for $w_1 \approx 0.16$ GeV/c. The H-dibaryon vertex, is parametrized as

$$\rho_H(\Delta p_H) = e^{-(\Delta p_H/w_H)^2}/w_H^2, \qquad (A4)$$

with $w_H = 0.73$ GeV/c, where the difference between the cascade momentum and that of the second proton, $\boldsymbol{p}_2$, is given by $\Delta p_H = \sqrt{(p_H^l - 2p_2^z)^2 + (p_H^\perp - 2p_2^x)^2 + (-2p_2^y)^2}$. The total energy of the recoiling nucleus is $\epsilon = [(p_r^l)^2 + (p_r^\perp)^2]/(2\,B\,m_p) + \beta$, where β is the binding energy, which is taken to be 0.008 GeV and $B = A - 2$. The H-dibaryon energy, E_H, is obtained from total energy conservation, $E_H = E_{K^-} - E_{K^+} + 2m_p - \epsilon$. The longitudinal and perpendicular components of $\boldsymbol{p}_H$ are labeled as p_H^l and $p_H^\perp$, respectively, and are calculated from the total momentum conservation, $p_H^l = p_{K^-} - p_{K^+} - p_r^l$, $p_H^\perp = -p_r^\perp$. The H-dibaryon mass
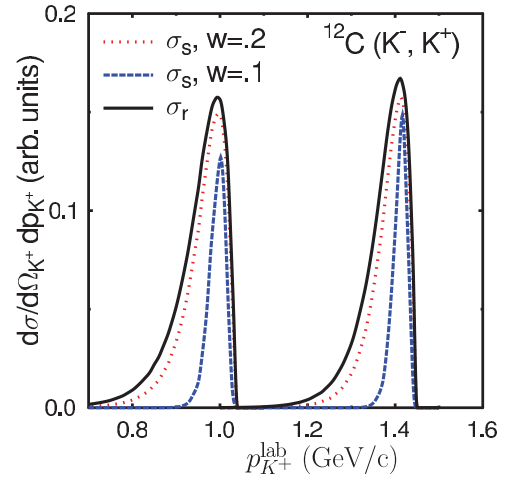

FIG. 8. (Color online) Cross sections calculated with simplified expressions given by Eqs. (A1) and (A5) for K^+ angles of $0°$ as a function of K^+ momentum in the laboratory system at $p_{K^-}^{lab}$ values of 1.4 and 1.8 GeV/c. The solid lines represent the results obtained with Eq. (A1) while the dashed and dotted lines represent those obtained with Eq. (A5) for $W = 0.1$ and 0.2 GeV, respectively. The absolute magnitudes of the cross section are arbitrary.

is set at $m_H = 2.2$ GeV. The perpendicular component of the recoil is obtained by solving the "on-shell" condition $m_H^2 = E_H^2 - p_H^2$.

In Fig. 8 the cross section obtained from Eq. (A1) is compared with that obtained from an even simpler expression,

$$\sigma_s(p_{K^+}) = \int dp_r^l \rho_s(p_r) \, p_r^\perp, \qquad (A5)$$

where the overlap integral is simplified to the extreme as

$$\rho_s(p_r) = e^{-(p_r/w)^2}/w^2. \qquad (A6)$$

In Fig. 8, we show the cross sections as a function of K^+ momentum in the laboratory system for $p_{K^-}^{lab}$ values of 1.4 and 1.8 GeV/c. The solid lines show the results obtained by using Eq. (A1) while dashed and dotted lines those obtained with Eq. (A5) for $W = 0.1$ and 0.2 GeV, respectively. First of all we note that the widths of the cross sections σ_R are very close to those of the cross sections shown in Figs. 5–7. Furthermore, for $W = 0.2$ GeV, the cross sections σ_S are very close to the cross sections σ_R. Thus this provides an excellent simple parametrization of the cross sections shown in Figs. 5–7. The width of the K^+ momentum distribution is narrower for smaller values of W. This is expected to be the case for the bound proton states in heavier targets.

[1] R. L. Jaffe, Phys. Rev. Lett. **38**, 195 (1977).
[2] K. F. Liu and C. W. Wong, Phys. Lett. B **113**, 1 (1982).
[3] P. J. Mulders and A. W. Thomas, J. Phys. G **9**, 1159 (1983).
[4] M. Oka, K. Shimizu, and K. Yazaki, Phys. Lett. B **130**, 365 (1983).
[5] T. Sakai, K. Shimizu, and K. Yazaki, Prog. Theor. Phys. Suppl. **137**, 121 (2000).
[6] C. J. Yoon *et al.*, Phys. Rev. C **75**, 022201(R) (2007).
[7] Neha Shah (STAR Collaboration), Act. Phys. Pol. Proc. Suppl. **5**, 593 (2012).
[8] H. Takahashi *et al.*, Phys. Rev. Lett. **87**, 212502 (2001); K. Nakazawa, Nucl. Phys. A **835**, 207 (2010).
[9] S. R. Beane *et al.*, Phys. Rev. Lett. **106**, 162001 (2011).
[10] T. Inoue *et al.*, Phys. Rev. Lett. **106**, 162002 (2011); Nucl. Phys. A **881**, 28 (2012).
[11] P. E. Shanahan, A. W. Thomas, and R. D. Young, Phys. Rev. Lett. **107**, 092004 (2011).

[12] J. Haidenbauer and U.-G. Meißner, Phys. Lett. B **706**, 100 (2011); Nucl. Phys. A **881**, 44 (2012).

[13] S. R. Beane, E. Chang, W. Detmold, B. Joo, H.-W. Lin, T. C. Luu, K. Orginos, A. Parreno, M. J. Savage, A. Torok, and A. Walker-Loud, Mod. Phys. Lett. A **26**, 2587 (2011).

[14] T. F. Carames and A. Valcarce, Phys. Rev. C **85**, 045202 (2012).

[15] J. K. Ahn *et al*., proposal "Search for H-Dibaryon with a Large Acceptance Hyperon Spectrometer," available at http://nuclpart.kek.jp/pac/1207/pdf/15thPAC.120714.P42.JKAhn.pdf.

[16] L. Guo *et al*., Phys. Rev. C **76**, 025208 (2007).

[17] R. Shyam, K. Tsushima, and A. W. Thomas, Nucl. Phys. A **881**, 255 (2012).

[18] R. Shyam, Nucl. Phys. A (2013), doi: 10.1016/j.nuclphysa.2013.01.082.

[19] P. A. M. Guichon, A. W. Thomas, and K. Tsushima, Nucl. Phys. A **814**, 66 (2008).

[20] C. B. Dover and A. Gal, Ann. Phys. (NY) **146**, 309 (1983).

[21] R. Shyam, O. Scholten, and A. W. Thomas, Phys. Rev. C **84**, 042201(R) (2011).

[22] A. T. M. Aerts and C. B. Dover, Phys. Rev. Lett. **49**, 1752 (1982).

[23] A. T. M. Aerts and C. B. Dover, Phys. Rev. D **28**, 450 (1983).

[24] N. Aizawa and M. Hirata, Z. Phys. A **343**, 103 (1992).

[25] A. T. M. Aerts and C. B. Dover, Phys. Rev. D **29**, 433 (1984).

[26] J. D. Bjorken and S. D. Drell, *Relativistic Quantum Mechanics* (McGraw-Hill, New York, 1964).

[27] R. Shyam, Phys. Rev. C **60**, 055213 (1999).

[28] R. Shyam, H. Lenske, and U. Mosel, Phys. Rev. C **77**, 052201(R) (2008).

[29] R. Shyam, H. Lenske, and U. Mosel, Phys. Rev. C **69**, 065205 (2004); Nucl. Phys. A **764**, 313 (2006)

[30] R. Shyam, K. Tsushima, and A. W. Thomas, Phys. Lett. B **676**, 51 (2009).

[31] S. Bender, R. Shyam, and H. Lenske, Nucl. Phys. A **839**, 51 (2010).

[32] F. Ajzenberg-Selove, Nucl. Phys. A **506**, 1 (1990).

[33] F. Ajzenberg-Selove, Nucl. Phys. A **490**, 1 (1988).

[34] R. Shyam, W. Cassing, and U. Mosel, Nucl. Phys. A **586**, 557 (1995).

[35] J. K. Ahn *et al*., Phys. Lett. B **378**, 53 (1996).

[36] K. Yamamoto *et al*., Phys. Lett. B **478**, 401 (2000).

[37] K. Ikeda, T. Fukuda, T. Motoba, M. Takahashi, and Y. Yamamoto, Prog. Theor. Phys. **91**, 747 (1994).

[38] C. B. Dover, A. Gal, and D. J. Millener, Nucl. Phys. A **572**, 85 (1994).

[39] Y. Yamamoto, T. Motoba, T. Fukuda, M. Takahashi, and K. Ikeda, Prog. Theor. Phys. Suppl. **117**, 281 (1994).